Johann Radon Institute for
Computational and Applied Mathematics
Austrian Academy of Sciences (ÖAW)

A numerical continuation approach for computing water waves of large wave height

D. Amann, K. Kalimeris

RICAM-Report 2017-09

A numerical continuation approach for computing water waves of large wave height

D. Amann and K. Kalimeris

Radon Institute for Computational and Applied Mathematics,
Austrian Academy of Sciences, Linz, Austria.

August 4, 2017

Abstract

We analyze an algorithm for the calculation of travelling water waves in flows with constant and variable vorticity. The algorithm is based on numerical continuation techniques, which are suitably adapted to the water wave problem. Numerical examples illustrate the performance of the algorithm for flows of constant vorticity, where the results are compared with the literature. We observe agreement with already existing results, but we also have some new qualitative and quantitative results considering the characteristics of the water waves both for constant and variable vorticity.

Keywords: Travelling water waves, vorticity, pressure, stagnation, numerical continuation.

1 Introduction

We are studying two-dimensional waves travelling at constant speed c, for different vorticities. This problem has practical interest because it is related with the detection of non-uniform underlying currents from the surface wave pattern. The characterization 'travelling' means that in a two-dimensional frame moving with the constant speed c, the flow pattern — and, in particular, the shape of the surface of the fluid — does not change over time. Two-dimensionality means that the waves propagate in a fixed horizontal direction and the flow presents no variation in the horizontal direction orthogonal to the direction of wave propagation. For this reason, it suffices to analyse a vertical cross-section of the flow, parallel to the direction of wave propagation. To model sea waves of large amplitude the assumptions of inviscid flow in a fluid of constant density are appropriate and the effects of surface tension are negligible – see the discussion in [11].

It is worth highlighting the physical importance of flows with vorticity in modelling wave-current interactions; general discussions of the physical implications of rotational flow may be found in the references [11] and [53]. Recent studies have pointed out that

periodic travelling waves which propagate at the surface of water with a flat bed in a flow of constant vorticity must be symmetric if no flow-reversal occurs and if the wave profile is monotone between successive crests and troughs, see [13, 14]. This means that an underlying non-uniform current of constant vorticity does not break the symmetry of irrotational wave trains. Thus, following this formulation, we make the assumption of no flow-reversal in this work: In the absence of flow reversal, the approach developed in [15] ensures the real-analyticity of all the streamlines; see also the discussion in the survey [29]. In contrast to this, the available results on regularity for flow reversal (case in which critical layers appear) are merely of class C^∞, see the results in [21].

Prior to the establishment of any analytically rigorous mathematical results, numerical investigations for large amplitude waves with vorticity, were initiated by the seminal papers [50] and [22] for the infinite, and finite, depth cases respectively. Indeed, due to significant technical complications, rigorous mathematical analysis establishing the existence of large amplitude water waves has only recently been achieved. In the case of irrotational waves this was achieved by the work of Toland and collaborators (where [6, 52] represent nice surveys of this topic), and for waves with vorticity, following the seminal paper [18], the existence of large amplitude waves was established for various physical generalisations in [33, 35, 43, 58].

In this work, we follow the analytical formulation derived in [18], and reviewed in several other works, see for example [51, 17]. In this approach, the curve of solutions is extensively analyzed and a crucial ingredient is the existence of a branch of the bifurcating diagram, which contains flows beneath genuine waves[1]. In particular, this branch starts from a special laminar solution, the existence of which is connected with the so-called *dispersion relation*; this curve may be continued, using arguments from bifurcation theory, to a global continuum which contains at the limit a flow with a stagnation point. The characteristic of the latter wave is that its horizontal velocity approaches the constant speed of propagation c, being related to waves of maximal amplitude, hence providing the analogue to the Stokes' extreme wave. Computations which are based on this approach are performed in [39, 38], with several interesting results which agree with the relevant analytical predictions. Among the most important results of those works we point out the following: The stagnation can occur, not only at the crest, but also at the point on the bottom directly below the crest. Along the bifurcation curve, for fixed relative mass flux[2] p_0, the amplitude of the wave is increasing, the depth d varies only slightly and the hydraulic head[3] Q has (in general) one turning point. Furthermore, the waves of maximal amplitude are obtained at the end of the bifurcation curve and the maximal amplitude is an increasing function of $|p_0|$, in the case of constant vorticity. Finally, the shapes of the streamlines of the extreme waves depend on the vorticity, which is a result observed also in several numerical works and indicates the importance of the effect that the vorticity has on the features of water waves.

In our work, we analyze a numerical continuation approach tailor-made for the above

[1] In the sense that they are not of zero amplitude.

[2] The flux p_0 is defined in (9).

[3] This quantity, being indicative of the total mechanical energy of the wave, is defined in (12).

described mathematical formulation, enriched with techniques appropriate to overcome some particular obstacles of this problem (turning points, bifurcation points and stagnation points). The idea on reconstructing the bifurcation branch described in [18], via numerical continuation techniques, was introduced in [39]. In our algorithm, among other techniques which are described in more detail in section 4, we make explicit usage of analytical results obtained in [18] — instead of evaluating numerically the relevant features, through the solution of an eigenvalue problem. In more detail:

- The explicit position of the bifurcation point, which is the starting point of our iterative numerical scheme is obtained analytically through [18], [17] and [37] for different cases of vorticity.

- Starting from the above point, the favourable direction for the numerical continuation, which will lead to the reconstruction of the branch containing the non-laminar flows (as opposed to the trivial one), is obtained analytically in [18], [16] and [37], for the different cases of vorticity.

- The careful refining of the mesh described in section 4 allows for the computation of waves closer to stagnation than the ones obtained in [39].

- The adaptation (described in section 3) of the numerical continuation technique on this formulation of the water wave problem allows the systematic study of the main features of the wave and the improvement of the algorithm; as examples we note the adaptation of the step-size in the 'predictor stage' of our method and the interchange of the continuation parameter.

This has as a result an efficient and inexpensive algorithm, which, additionally, gives rise to new parts of the interesting branch of the bifurcation diagram, i.e. to families of waves with novel characteristics, see for example Section 4.2. Furthermore, we find agreement with already existing numerical results while observing additional characteristics close to stagnation, which in some cases is important enough to give an additional understanding on the solutions of the problem. Finally, in order to show the generality of our algorithm, we compute some cases of continuous and non-constant vorticity; this results in, also, an interesting family of water waves, which is depicted in Figures 23-24.

We find worth-mentioning a series of computational works, for example [45, 55, 56, 46, 32], which are based on a different mathematical formulation of the problem. In particular, they are based on the analysis of [23, 2]; see also [4, 31] and [30] for extending the latter work in a domain with fixed and moving bottom, respectively. One can observe that our computational results are in qualitative agreement with results of the above-mentioned works.

In the recent work [47] an extensive numerical study of periodic travelling water waves is made. This work is based on a conformal mapping which is described also in [7, 44] and their results are obtained through a combination of analytical techniques and spectral methods. This approach has the advantage over our work that the computation of waves with stagnation points (both on the boundary and in the interior) are possible.

On the other hand this approach treats only the case of constant vorticity; one could find potential on extending this work to general vorticity using the analysis of [57] and [27]. Our approach, although having the disadvantage on stagnation points, provides results for more general distributions of vorticity; as an example we provide some examples in section 4.3. Moreover, our computation reveals some interesting behaviour of the pressure for a particular family of waves which is discussed in Section 4.2 and it is novel, up to our knowledge. Even though that for waves that do not have stagnation points there is qualitative agreement between our work and the above-mentioned one, the most interesting cases of that work involves waves with internal stagnation (which we do not compute). Finally, the rigorous and *exact* correspondence of these two formulations – the conformal mapping used in [47] and the semi-hodograph transformation used in [18] and here – is still an open question.

The paper is organised as follows: In section 2, we make a brief review of the mathematical formulation of the problem. In section 3, we present the numerical continuation method, which we employ in order to compute the water waves along the bifurcating curves. In section 4, we present the numerical results of the above procedure and we discuss the special characteristics of the waves, depending on the different values of constant vorticity. Moreover, in order to show the generality of our algorithm, we present the relevant results for some case that the vorticity is not constant; in these examples the vorticity varies linearly, as well as quadratically, with respect to the stream function. In particular, we illustrate the wave profiles, as well as other characteristics such as the velocity profile and the pressure throughout the fluid. The knowledge of these flow characteristics is very useful in qualitative studies, see [10, 20]. Moreover, in practice information on the state of the sea surface is often gathered from subsurface pressure and/or velocity measurements; we refer to the discussions in [8, 9, 12, 33, 40, 46].

2 The basic equations and terminology

In this section we present the governing equations for periodic two-dimensional travelling water waves in flows of constant and variable vorticity over a flat bed.

Let us denote the height function of the wave above the flat bottom by $h(q,p)$. This function satisfies the nonlinear boundary value problem, defined by (1)-(3). We omit here the derivation of (1)-(3) from the physical problem which was described in the Introduction. Instead, for the derivation of the constitutive equations (1)-(3) and the mathematical formulation of the problem we refer to [18, 51] for a detailed construction, to [17, 39] for an extended review and to [16, 36] for a brief review.

Definition 1. *The constitutive equations for the height function $h(q,p)$, which is even and $2L$-periodic in q, are the following:*

$$(1+h_q^2)h_{pp} - 2h_p h_q h_{qp} + h_p^2 h_{qq} - \gamma(-p)h_p^3 = 0 \quad \textit{in } R, \tag{1}$$

$$1 + h_q^2 + (2gh - Q)h_p^2 = 0 \quad \textit{for } p = 0, \tag{2}$$

$$h = 0 \quad \textit{for } p = p_0, \tag{3}$$

where R is the rectangle defined by

$$R = \{(q,p) : \ -L < q < L, \ p_0 < p < 0\}. \tag{4}$$

Moreover, the free boundary of the wave is given by the expression $h(q,0)$.

In this equation γ denotes the vorticity as defined in (7), which is assumed a known function, being indicative of underlying currents. Vanishing vorticity is the property typical of uniform currents and a constant vorticity characterizes linearly sheared currents. We also recall that g is the gravitational constant of acceleration, and p_0 is the relative mass flux as defined in (9), and it is a constant, too. The parameter Q is called the hydraulic head, it plays an important role in the profile of the waves, and is defined in (12).

For the justification of the q evenness and periodicity of the water waves we refer to the discussion in [13, 14]. Moreover, without loss of generality, me make the assumption that the crest is at $q = 0$ and the trough at $q = L$. Thus, we define the wave height as the maximal variation of the oscillations of the free surface, given by

$$a := \max_{q\in[-L,L]} h(q,0) - \min_{q\in[-L,L]} h(q,0) = h(0,0) - h(L,0). \tag{5}$$

Following the methodology of [36], below we provide the sufficient terminology for the fundamental boundary value problem (1)-(3).

Basic terminology

In the description of the physical problem in the Introduction, we emphasized the fact that we are studying two-dimensional waves travelling at constant speed c. Moreover, we made the assumption of no flow-reversals and no surface tension.

We denote:

- The free boundary of the wave by

$$S = \big\{(x,y) : -L < x < L \text{ and } y = \eta(x)\big\},$$

- The flat bottom by

$$B = \big\{(x,y) : -L < x < L \text{ and } y = -d\big\},$$

with $d > 0$, for the normalized wavelength $2L$.

- The velocity field of the flow by

$$(u(x,y), v(x,y)),$$

with $(x,y) \in \mathcal{D}$, where

$$\mathcal{D} = \{(x,y) : -L < x < L \text{ and } -d < y < \eta(x)\}.$$

- The pressure in the fluid by $P(x,y)$, with $(x,y) \in \mathcal{D}$. Neglecting the effects of surface tension we impose that the water pressure is constant on S, $P(x,\eta(x)) = P_{atm}$, where P_{atm} is the atmospheric pressure.

The assumption of no flow-reversals, which also excludes stagnation point throughout the fluid domain, is formulated as the condition

$$u < c \quad \text{throughout the fluid.} \tag{6}$$

Let us recall the following definitions:

- The vorticity of the flow is defined by

$$\gamma := u_y - v_x. \tag{7}$$

Furthermore, we define the following function

$$\Gamma(p) := \int_0^p \gamma(-s)ds, \tag{8}$$

which is useful for describing other quantities of the problem.

- The relative mass flux[4] is defined by

$$p_0 := \int_{-d}^{\eta(x)} (u(x,y) - c)\, dy < 0, \tag{9}$$

which in fact is independent of x, see [17]. Moreover, condition (6) shows that p_0 is negative. This relation shows that the amount of water passing any vertical line is constant throughout $\mathcal{D}$.

- The stream function $\psi(x,y)$ is defined as the unique solution of the differential equations

$$\psi_x = -v, \qquad \psi_y = u - c \text{ in } \overline{\mathcal{D}}, \tag{10}$$

subject to

$$\psi(x,-d) = -p_0\,. \tag{11}$$

[4]The terminology 'relative' is due to the fact that $(u-c)$ is the relative horizontal velocity of the flow, with reference to the moving frame at speed c.

- The hydraulic head, which is *constant* throughout the fluid, and denoted by Q, is defined by

$$Q := (u-c)^2 + v^2 + 2g(y+d) + 2(P - P_{atm}) + 2\Gamma(-\psi), \tag{12}$$

where Γ was defined in (8). Indeed, it is proven in [18] and in [17], that the expression

$$\frac{(u-c)^2 + v^2}{2} + gy + P + \Gamma(-\psi)$$

is a constant throughout $\mathcal{D}$, thus the expression in (12) is constant, too; this is a form of conservation of energy.

The Dubreil-Jacotin transformation, see Figure 1, maps the unknown domain $\mathcal{D}$ to the rectangle R, defined in (4). The independent variables as they appear in the Dubreil-Jacotin transformation [25] are

$$q = x, \qquad p = -\psi.$$

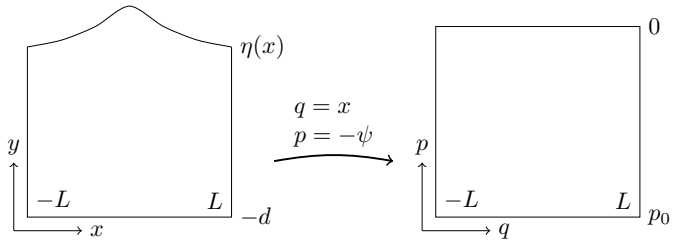

Figure 1: Dubreil-Jacotin transformation

Finally, we recall that:

- The height function $h(q,p)$ is defined by

$$h := y(q,p) + d, \tag{13}$$

where y is assumed to depend implicitly on new semi-Lagrangian $q,p-$variables.

- The velocity field is given by

$$(c-u, v) = \left(\frac{1}{h_p}, -\frac{h_q}{h_p}\right). \tag{14}$$

- The water pressure is given by

$$P = P_{atm} - \frac{1+h_q^2}{2h_p^2} - gh - \Gamma(p) + \frac{Q}{2}, \tag{15}$$

with Γ being defined in (8).

- The coordinates are chosen such that the mean-water level is located at $y = 0$; then $\int_{-L}^{L} \eta(x)dx = 0$ and accordingly, from the definition of h, the mean-depth of the fluid is recovered by the expression

$$d = \frac{1}{2L}\int_{-L}^{L} h(q,0)dq. \tag{16}$$

Remark 1. *The mean-depth of the fluid can only be recovered a posteriori following bifurcation from the standard Dubreil-Jacotin formulation of the water wave problem – indeed, in [39] it was shown that the depth d varies along the bifurcation continuum; similar results are presented also here in Figure 15.*

A novel approach to overcome this issue was initiated in [33, 34]. Based on this formulation one may proceed through a similar numerical continuation technique and compute families of non-laminar water waves of fixed depth, where the relative mass flux p_0 will be varying. We consider this a very fruitful approach in order to see, among other interesting features, how the variation of the quantity p_0 will affect important characteristics of waves. In our opinion, a systematic numerical study of this formulation, can be presented independently of the current work and certainly deserves an article of similar length of this one. Recalling that in our computations, waves of maximal amplitude are obtained at the limiting points of the bifurcation curve, we observe that maximal amplitude increases as $|p_0|$ increases. For a brief overview on the influence of p_0 on the wave characteristics we refer to Remark 2 in Section 4.2.

3 Numerical Continuation

Discretization of (1)–(3) leads to a system of nonlinear equations

$$F(\theta, \mathbf{h}) = \mathbf{0} \tag{17}$$

with a given mapping $F : \mathbb{R}\times\mathbb{R}^N \to \mathbb{R}^N$ and unknowns $\mathbf{h} \in \mathbb{R}^N$ and $\theta \in \mathbb{R}$. To overcome the two major problems in solving (17), the underdetermined system and the need for a good initial guess, we employ a numerical continuation strategy. We consider the case that at least one solution is known and the goal is to compute additional solutions. Parametrization of the solution curve and fixing the step size results in a well defined problem and the known solutions are used to predict an initial guess. As a corrector we use a Newton algorithm to solve the system of nonlinear equations.

This section gives a short introduction into this topic, putting it in a more general frame, but also giving some specific details of the problem, where needed. For a more elaborate study we refer to [3, 24].

3.1 Predictor Corrector method

Let $\mathcal{C}$ be the set of all pairs satisfying (17) and $(\theta_k, \mathbf{h}_k) \in \mathcal{C}$ a known solution, then the problem is to find a new solution

$$F(\theta_{k+1}, \mathbf{h}_{k+1}) = \mathbf{0}.$$

Since this is an underdetermined system we first have to find an additional equation. Assume that a parametrization of the solution curve $\mathcal{C}$ in a neighbourhood of $(\theta_k, \mathbf{h}_k)$ is given such that

$$\begin{aligned} F(\theta(s), \mathbf{h}(s)) = 0 \quad &\text{for } |s| < s_0, \\ \theta(0) = \theta_k \quad \text{and} \quad &\mathbf{h}(0) = \mathbf{h}_k, \end{aligned}$$

for some $s_0 > 0$. Using the equation $\mathfrak{p}(\theta, \mathbf{h}, s) = 0$ to describe the above parametrization, we can append this to (17) for a fixed step size s resulting in

$$\begin{pmatrix} F(\theta_{k+1}, \mathbf{h}_{k+1}) \\ \mathfrak{p}(\theta_{k+1}, \mathbf{h}_{k+1}, s) \end{pmatrix} = \begin{pmatrix} \mathbf{0} \\ 0 \end{pmatrix}. \tag{18}$$

The existence and uniqueness of a solution to (18) depends on the choice of $\mathfrak{p}$ and the solution set $\mathcal{C}$. We now discuss two choices for $\mathfrak{p}$ and properties of the resulting systems.

Parametrization of $\mathcal{C}$ by θ is called natural parametrization and equates to fixing the value of θ. The corresponding function is

$$\mathfrak{p}(\theta, \mathbf{h}, s) = \theta - (\theta_k + s). \tag{19}$$

In a similar way, instead of θ we can choose any entry of $\mathbf{h}$ as parameter. Let i be an index of $\mathbf{h}$, then the so called local parametrization is given by

$$\mathfrak{p}(\theta, \mathbf{h}, s) = \mathbf{h}[i] - (\mathbf{h}_k[i] + s).$$

Figure 2 shows both these parametrizations on a bifurcation diagram that plots $(\theta, \mathbf{h}[i])$ for all solutions in $\mathcal{C}$. Additionally to $\mathcal{C}$ the line of all pairs $(\theta, \mathbf{h})$ satisfying $\mathfrak{p}(\theta, \mathbf{h}, s) = 0$ is also plotted, the solution we seek is the intersection of these two lines. The existence and uniqueness of such an intersection depends on $\mathcal{C}$ and the choice of s. In the example $\mathcal{C}$ has a turning point in θ, so there exists no solution pair that satisfies the natural parametrization if s is too large. Indeed, if the current solution is exactly on the turning point, there exists no $s_0 > 0$ such that (19) describes a parametrization of $\mathcal{C}$. In such a case, one way to proceed with the numerical continuation is by parametrizing with respect to another characteristic such that the bifurcation curve does not have a turning point, in the given example $\mathbf{h}[i]$.

For our model problem (1)–(3) it proved most effective to parametrize by the entry of $\mathbf{h}$ corresponding to the highest point of the wave. The considered solution curves $\mathcal{C}$ are monotonous in this parameter and thus have no turning points with respect to this parametrization.

The predictor is the initial guess for the Newton scheme and will be denoted as $(\theta_{k+1}^{(0)}, \mathbf{h}_{k+1}^{(0)})$. Of the many predictors described in literature we only briefly introduce two, the trivial and secant predictor

$$\begin{aligned} (\theta_{k+1}^{(0)}, \mathbf{h}_{k+1}^{(0)}) &:= (\theta_k + s^{(0)}, \mathbf{h}_k), \\ (\theta_{k+1}^{(0)}, \mathbf{h}_{k+1}^{(0)}) &:= (\theta_k, \mathbf{h}_k) + s^{(0)}(\theta_k - \theta_{k-1}, \mathbf{h}_k - \mathbf{h}_{k-1}). \end{aligned}$$

The value $s^{(0)}$ is chosen such that the parametrization equation is satisfied.

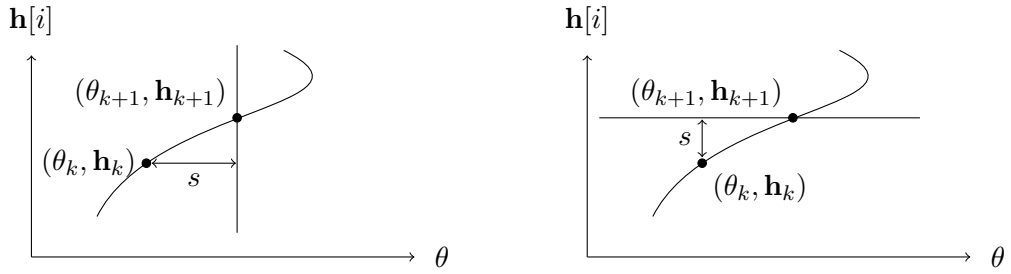

Figure 2: Natural and local parametrization

3.2 Bifurcation and turning points

Along the solution curve $\mathcal{C}$, two kind of points are of special interest. A turning point is illustrated in Figure 2 and means that locally there are two solutions below some value of θ and none above or vice versa. A point along $\mathcal{C}$ where two or more solution branches intersect is called a bifurcation point.

Let $(\theta_k, \mathbf{h}_k)$ be a solution of (17). The point is called regular if the Jacobian $(F_\theta | F_{\mathbf{h}}) \in \mathbb{R}^{N \times N+1}$ has full rank N. Near a regular point, $\mathcal{C}$ can be uniquely described by a one dimensional branch of solutions [24].

The full rank condition implies that at a regular point it must hold either $\operatorname{rank}(F_{\mathbf{h}}) = N$ or $\operatorname{rank}(F_{\mathbf{h}}) = N - 1$ and $F_\theta \notin \operatorname{range}(F_{\mathbf{h}})$. In the first case the branch of solution near $(\theta_k, \mathbf{h}_k)$ can be parametrized by θ [3]. The second case describes the situation of a turning point in θ, so even though $\mathcal{C}$ can be uniquely parametrized, θ is not the proper parameter. At last, if a point is not a regular point, then at least two branches of solutions intersect at this point.

While traversing along the bifurcation curve, it is important not to miss bifurcation points, we restrict our considerations to simple bifurcation points. For this we define a test function τ with the properties that $\tau(\theta^*, \mathbf{h}^*) = 0$ on a bifurcation point and $\tau(\theta^+, \mathbf{h}^+)\tau(\theta^-, \mathbf{h}^-) < 0$ if the two points are separated by a bifurcation point. One choice for a test function is the sign of the determinant of the Jacobian

$$\tau(\theta, \mathbf{h}) := \operatorname{sign}\left(\det\left(F'(\theta, \mathbf{h})\right)\right),$$

which is readily available if the linear system appearing in the Newton algorithm is solved via LU–decomposition. This and other test functions, such as the eigenvalue of smallest magnitude, are discussed in [49].

3.3 Bifurcation from the laminar flow

The numerical continuation method assumes that at least one solution of (17) is given. How to find this solution is problem–dependent and often includes a certain choice for the value of θ to facilitate the solution of the resulting system. Here we discuss how this can be done for the equations (1)–(3) arising from traveling water waves.

First we consider solutions H that are q-independent and correspond to parallel shear flows. These solutions $H(p)$ are called laminar waves and solve

$$\begin{aligned} H_{pp} - \gamma(-p)H_p^3 = 0 \quad & \text{in } R, \\ 1 + (2gH - Q)H_p^2 = 0 \quad & \text{for } p = 0, \\ H = 0 \quad & \text{for } p = p_0. \end{aligned}$$

For general vorticity, the laminar flow is given by

$$H(p;\lambda) = \int_{p_0}^{p} \frac{1}{\sqrt{\lambda - 2\Gamma(s)}} ds,$$

where λ satisfies the relation

$$Q = \lambda + 2g \int_{p_0}^{0} \frac{dp}{\sqrt{\lambda - 2\Gamma(p)}},$$

with Γ defined by (8). For some vorticity functions, for example $\gamma(p)$ constant or linear, solutions of this system are known analytically [16, 18, 37].

The above formulae give, not only one, but many solutions, in particular, we define the curve that contains the laminar flows

$$\mathcal{T} = \{(Q(\lambda), H(p;\lambda)) : \lambda > 0\}.$$

However, if we are to compute nonlaminar solutions, we need more information. Indeed, in [18] it was proven that near this curve, as the parameter λ varies, there are generally no genuine waves, except at some critical values $\lambda = \lambda_*$, which can be determined by the following procedure.

Define the linearized height function $h_L = H + bm$ with $b \in \mathbb{R}_+$ and m chosen such that h_L solves (1)–(3) up to an error of order $\mathcal{O}(b^2)$. This leads to the linearized system

$$\begin{aligned} m_{pp} + H_p^2 m_{qq} = 3\gamma H_p^2 m_p \quad & \text{in } R, \\ gm = \lambda^{3/2} m_p \quad & \text{for } p = 0, \\ m = 0 \quad & \text{for } p = p_0, \end{aligned}$$

with the appropriate periodicity conditions in the q variable. For general values of $\lambda > 0$ the linearized system will only have the trivial solution $m \equiv 0$. In order to obtain non-trivial solutions $m(q,p)$ of the above system we make usage of the so-called 'dispersion relation'; for the water waves this is a consistency relation which is determined by the critical bifurcation values of the parameter $\lambda = \lambda_*$, see [11, 18]. For some choices of vorticity, including constant and linear, the dispersion relation as well as analytical forms for m are known [16, 37]. Moreover, in [18] it was proven that $(Q(\lambda_*), H(p;\lambda_*))$ is a bifurcation point on the curve $\mathcal{T}$, from where a curve that contains non-laminar flows arises, with Q being the global bifurcation parameter. This reads as a mapping $Q \mapsto h(q,p;Q)$ such that $h_q \not\equiv 0$ unless $h = H(p;\lambda_*)$. Furthermore, this curve may

be continued, using arguments from analytic global bifurcation theory [6], to a global continuum which contains at the limit a flow with a stagnation point; such a flow is analogous to the Stokes' wave of greatest height, or Stokes' extreme wave, in the irrotational setting [6, 11]; we denote the value of the bifurcating parameter at this flow by $Q = Q_M$.

Let b be fixed, then h_L is a predictor for a solution on the bifurcation branch. Note that a too small b will urge the corrector to converge to a laminar wave while a too big b can result in a diverging corrector step. In our experience, the choice $b = s$ with a small enough s leads to convergence to the nonlaminar branch.

Higher than first order approximations for h are known [16, 36] but a first order expansion is sufficient to bifurcate from the curve of laminar flows.

4 Numerical results

For the numerical examples, we fix the values of the parameters

$$g = 9.8, \qquad L = \pi, \qquad \text{and} \qquad p_0 = -2.$$

This choice of parameters is made accordingly to the one in [38]; we make this choice for allowing the comparison with the results displayed therein. From the particular choice of parameters the one that is of interest is the choice of the value of the relative mass flux p_0. We refer to the discussion in Remarks 1 and 2, for the influence of the choice of other values of p_0.

As in [38, 39] we discretize the system (1)–(3) by a second order finite difference scheme resulting in a system of nonlinear equations of the form (17). Instead of discretizing the whole domain $[-\pi, \pi] \times [p_0, 0]$ we exploit that h is an even function and only consider $[-\pi, 0] \times [p_0, 0]$, reducing the computational cost. In the interior and at the boundary $q = -\pi$, we used central schemes to approximate the derivatives of h. In order to be able to do this we expanded the solution beyond the left border by mirroring along $q = -\pi$. This procedure was motivated by the periodicity of h and the expected regularity at $q = -\pi$. At the border $q = 0$ such regularity assumptions are not satisfied, in particular close to a stagnation point, so we used backward difference schemes in q and a central scheme in p. Vice versa, we used a forward scheme in p and a central scheme in q on the top of the boundary.

The described algorithm was implemented using PETSc [5] for assembling and solving the non-linear systems. The computational domain is discretized by a equidistant 400×400 grid and then additionally refined where stagnation points and thus weaker regularities are expected. From theoretical [19] and numerical [38, 39] results and tests with equidistant grid points we know that the first encountered stagnation point is below the crest of the wave either on the top or on the bottom. To account for both these cases, we refine at the top and the bottom which results in a mesh with 460×580 grid points. At the expected stagnation points the mesh size is 8 times smaller than it was for the equidistant grid.

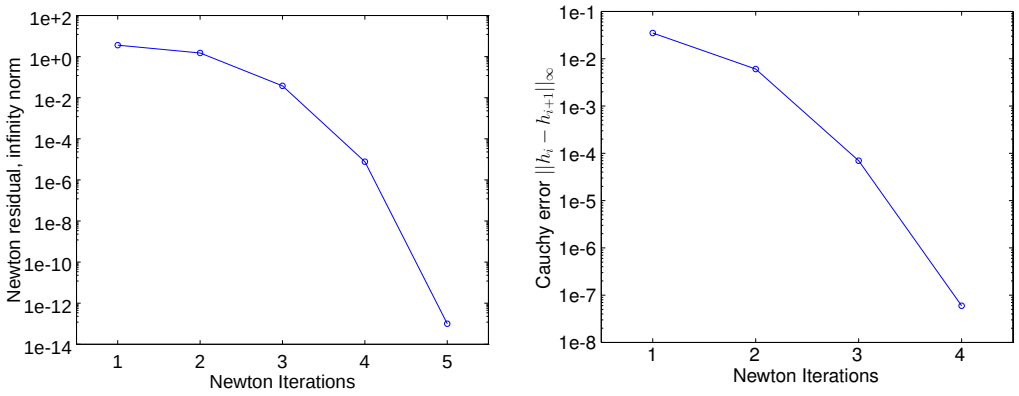

(a) Cost functional (b) Cauchy error

Figure 3: Newton Iterations.

Moreover, for the case of constant vorticity, in [38, 39], a critical (numerical) value of the parameter γ appears, denoted as γ_{crit}, which distinguishes the above two cases. In particular, if $\gamma > \gamma_{\text{crit}}$ the stagnation point appears in the top, whereas, if $\gamma < \gamma_{\text{crit}}$, the stagnation point appears at the bottom of the fluid[5]. The computed waves, in this section, demonstrate different characteristics below and above a critical vorticity which is, for the above choice of parameters, $\gamma_{\text{crit}} \approx -2.971$. We emphasize the fact that we obtain, also, some new qualitative results, compared with [38]; these are discussed in Section 4.2.

The natural choice for the bifurcation parameter θ is Q when we assume all other parameters to be fixed. For most of our computations we used this parameter. Note that for waves of constant vorticity we can alternatively fix Q and choose γ to be the bifurcation parameter. This choice can be beneficial and we will discuss one such case in Section 4.2.

Considering the validation of our algorithm, we first illustrate the performance of the corrector step to solve (18), for which we employ a Newton algorithm and stop when the residual is below 10^{-12}. Figure 3 shows for one exemplary wave the residual of the cost function (18) and the Cauchy error where we compare two solution of two successive Newton steps. We note that this strategy is in accordance with the common practice in the error analysis of this problem, see for example [56]. Furthermore, we have performed the same error tests for some example (laminar flow), for which we have the a priori knowledge of the analytical expression of the solution. The results show the same behaviour of our algorithm as in Figures 3.

The number of necessary Newton steps depends on various factors, mainly the predictor model and the step size. We used the secant predictor which reduced the necessary Newton steps in contrast to the trivial predictor in most cases by one to two. While

[5]Here, we have taken into consideration the difference of the sign of the vorticity between the above references and our work.

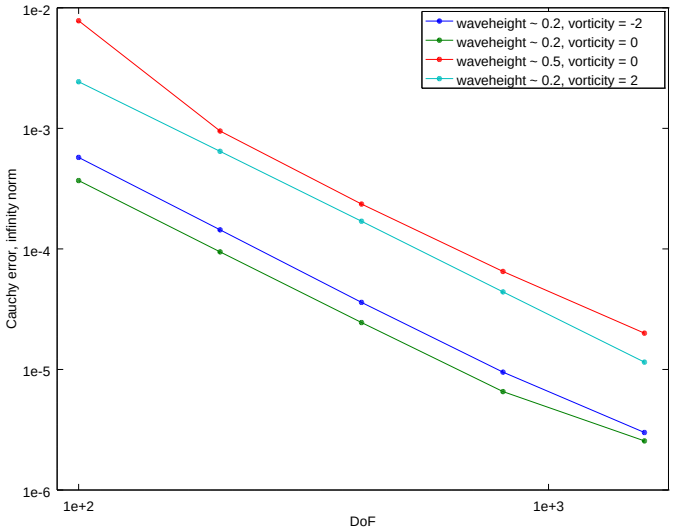

Figure 4: The Cauchy error $||h_N - h_{N/2}||_\infty$ for several vorticities and wave heights.

smaller step sizes decrease the necessary Newton iterations, the need for more predictor-corrector steps far outweighs the savings in Newton steps. On the other hand, too large step sizes can lead to a diverging corrector step, either because of a bad initial guess or an unsolvable system. One strategy that works well for most computations is an initial step size $s \approx 0.1$ which is multiplied by a factor $\frac{1}{3}$ if the corrector step does not converge. The number of necessary Newton steps for the presented results is between 4 to 6 once on the non-laminar branch and 7 to 9 for the bifurcation from the laminar branch.

Figure 4 shows the Cauchy error for different values of constant vorticity and wave height. Here the Cauchy error is the difference of two solutions h_N and $h_{N/2}$ where the sub index denotes the degrees of freedom used to discretize the free boundary. A decreasing Cauchy error indicates that the computed approximation is mesh independent. We see that the Cauchy error behaves similarly for all four considered cases and only varies in the absolute value. Note that for the irrotational case ($\gamma = 0$) the wave height 0.5 is already 97.7% of the maximal observed wave height and close to the stagnating wave.

These results support the claim that the algorithm presented in [39, 38], which our work is based on, provides a reliable way to compute waves of large amplitude and our improvements, like finer grading of the mesh, lead to a better approximation, thus allowing for computations closer to stagnating waves. Choosing the residual threshold 10^{-12}, in accordance[6] with other numerical studies on water waves [41, 42], ensures that solving the non-linear system does not introduce dominant errors. Being not the main scope of this work to present an algorithm performing with substantially better accuracy on computing the well studied (irrotational) Stokes' wave, we construct an

[6]The deviation of the Bernoulli constant in [41] is of the order 10^{-10} while in our computations it is of order 10^{-12}.

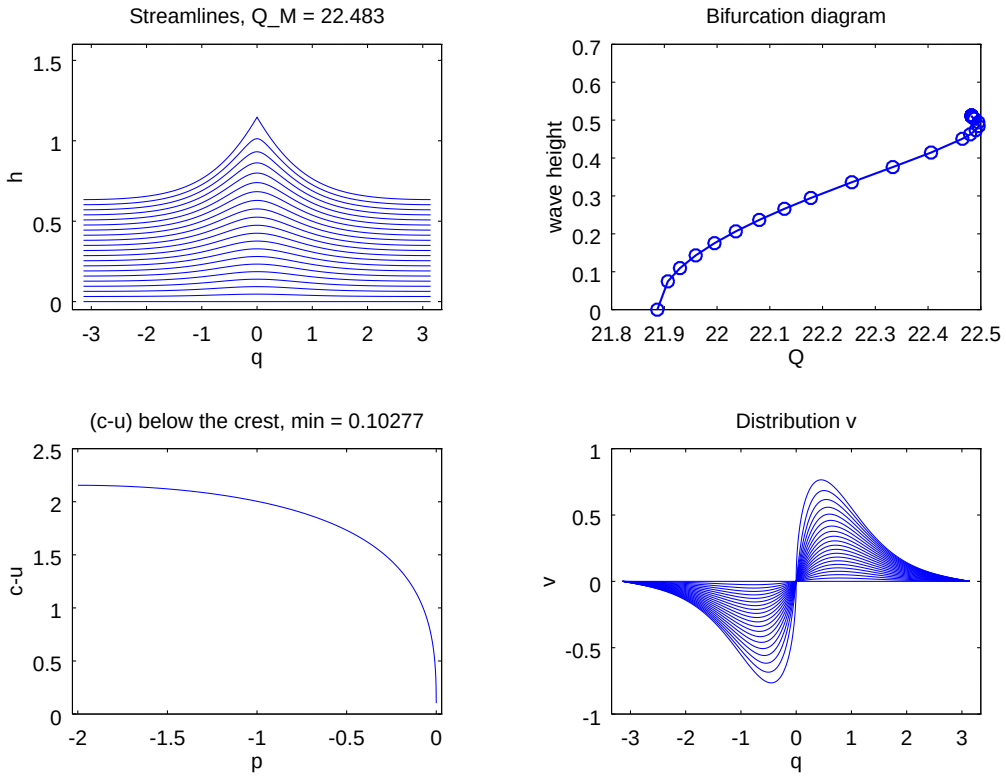

Figure 5: The Stokes' wave for $\gamma = 0$ (obtained at $Q = Q_M$) and its bifurcation diagram.

algorithm which improves on [39, 38] and is quite general in the computation of waves with non-constant vorticity.

4.1 Vorticity above the critical value

Recall that the linearized height function

$$h_L(q,p) = H(p) + bm(q,p)$$

is, for a proper step size $b = s$, a predictor for a solution on the non-laminar branch.

Referring to [18, 36], for constant vorticity,

$$\gamma(-p) \equiv \gamma,$$

the laminar solution is given by

$$H(p) = \frac{2(p-p_0)}{\sqrt{\lambda_* - 2\gamma p} + \sqrt{\lambda_* - 2\gamma p_0}}, \quad p_0 \le p \le 0,$$

where λ_* satisfies the dispersion relation

$$\frac{\lambda}{g - \gamma\sqrt{\lambda}} + \tanh\left(\frac{2p_0}{\sqrt{\lambda} + \sqrt{\lambda - 2p_0\gamma}}\right) = 0.$$

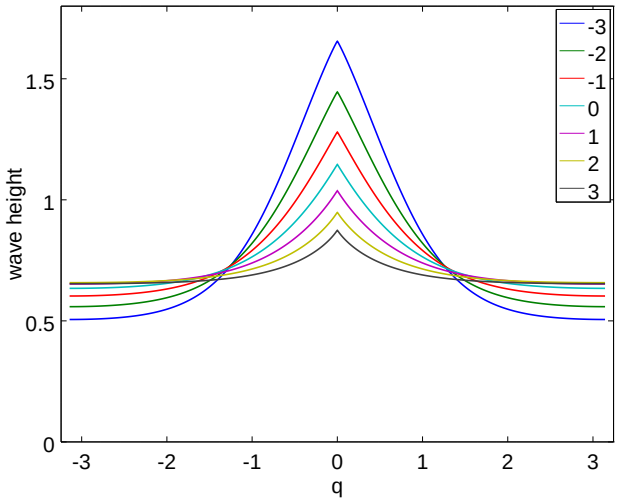

Figure 6: The free boundary of maximal waves (obtained at $Q = Q_M$) for different values of constant vorticity.

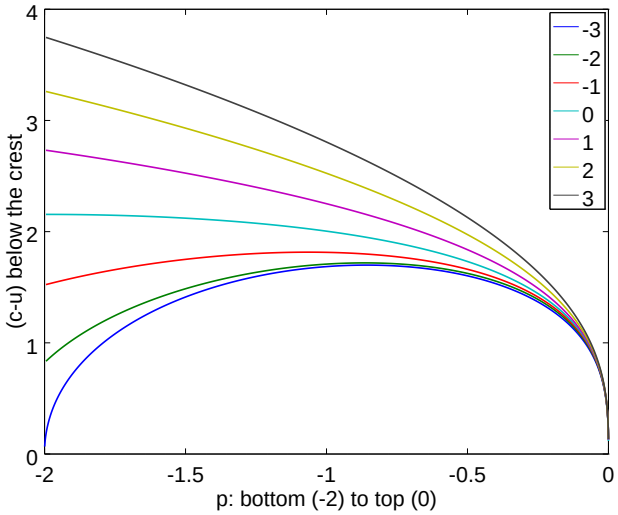

Figure 7: For different values of constant vorticity: The horizontal part, $(c - u)$, of the velocity field, on the vertical line below the wave crest, for maximal waves (obtained at $Q = Q_M$).

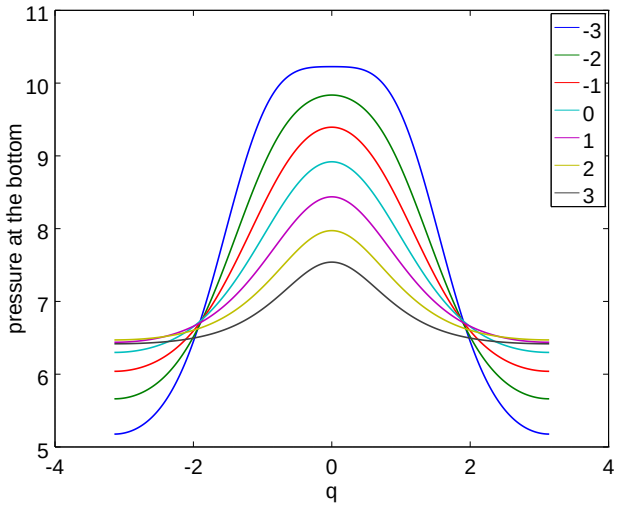

Figure 8: For different values of constant vorticity: The pressure at the flat bottom , for maximal waves (obtained at $Q = Q_M$).

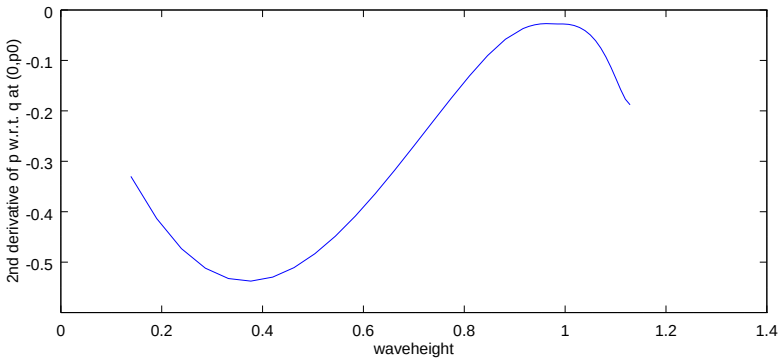

Figure 9: The value of $P_{qq}(0, p_0)$ along the bifurcation curve for $\gamma = \gamma_{\text{crit}}$.

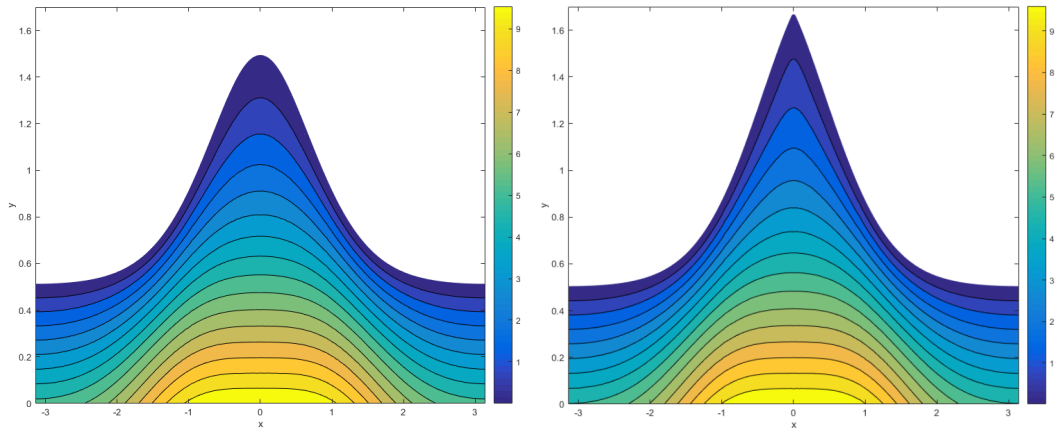

(a) $\gamma = \gamma_{\text{crit}}$ at Q_G (b) $\gamma = \gamma_\ell$ at Q_M

Figure 10: Contourplot of the pressure in the physical domain.

Furthermore, the function $m(q,p)$ is given by

$$m(q,p) = \frac{\sqrt{\lambda_* - 2p_0\gamma}}{\sqrt{\lambda_* - 2p\gamma}} \sinh\left(H(p)\right) \cos q, \qquad p_0 \le p \le 0, \quad -\pi \le q \le \pi.$$

Thus, now, we can perform the numerical continuation approach that was described above, using as an initial guess the linearized height function. For $\gamma > \gamma_{\text{crit}}$ the first observed stagnation point appears at the top of the wave. Such a stagnation point breaks the proposed algorithm since it violates the assumption $c - u > 0$ and leads to weaker regularity of h. As a stopping indicator we choose the minimum of $c - u$ which measures how close to a stagnation we are. We denote a wave as a stagnating wave once $c - u$ reaches 5% of its initial value at the laminar wave H. The magnitude of this threshold is in accordance with the literature, and in general smaller in our computation, allowing us to compute waves closer to stagnation and of larger wave height. We recall here, that once the profile of the wave $h(q,p)$ is computed, then the quantity $c - u$ is readily available by equation (14).

Since all waves for $\gamma > \gamma_{\text{crit}}$ show the same characteristic we only discuss one example in detail and give some remarks on the influence of γ. Figure 5 shows the famous Stokes' wave of greatest height, i.e. the limiting wave for $\gamma = 0$, which is obtained for $Q = Q_M$. At first we present a plot of the streamlines, which show the characteristic 120° degree angle occurring at the stagnation point at the wave crest; each streamline is defined by $[p = \text{constant}]$, with this constant taking values in the interval $[p_0, 0]$. With the same technique, we depict v, which is the vertical part of the velocity field, given by (14). Finally, we plot the bifurcating curve $\mathcal{C}$ for which we observed two turning points in Q, which is a novel characteristic of $\mathcal{C}$. It is interesting that the second picture in Figure 5 concurs with a quite surprising conjecture stating that, of all regular irrotational waves,

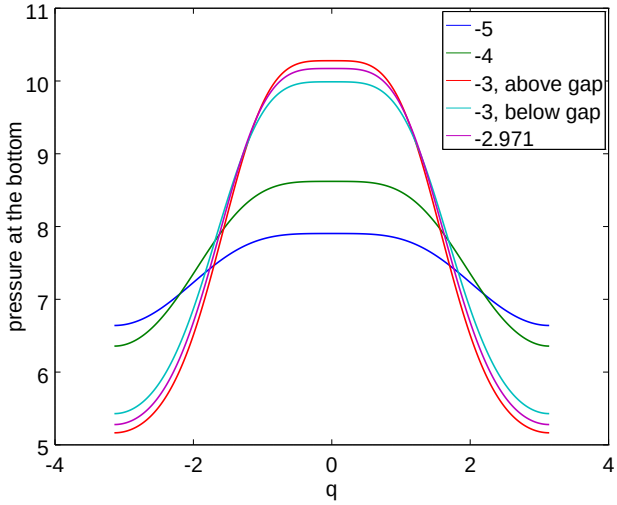

Figure 11: Pressure at the flat bottom for the maximal wave of $\gamma = -4, -5$, directly below and above the gap for $\gamma = -3$ and Q_G for $\gamma = \gamma_{\text{crit}} = -2.971$.

whereas the wave of greatest height is indeed the highest travelling wave, it does not actually maximise other physical quantities inherent to such waves: it is not the fastest, or most impulsive, or most energetic (as represented here by Q). This was also first observed by way of numerical investigations, cf. [48].

The appearance of two turning points in Q and a monotonously increasing wave height along the solution curve is observed for all constant vorticities $\gamma > \gamma_{\text{crit}}$. The value of γ does have a significant influence on the stagnating waves. Indeed, in Figure 6 we present the profiles for the waves of maximal amplitude which are obtained for the value of hydraulic head $Q = Q_M$. We observe the following characteristics for the wave profile:

- The wave height decreases, as the vorticity γ gets larger.
- The shape of the wave changes with the vorticity; the crest becomes sharper and the trough wider and flatter as the vorticity increases. For some interesting rigorous mathematical treatment of extreme waves, or wave with stagnation points, which possess an underlying vorticity we refer to [19, 54].

Furthermore, in Figure 7 we present the results for the speed $(c-u)$ below the crest, for the maximal waves obtained for each value of constant vorticity and whose wave profiles were presented in Figure 6, respectively; these results display qualitatively different distribution of the speed $(c-u)$ below the crest, which becomes more transparent closer to the bottom of the flow.

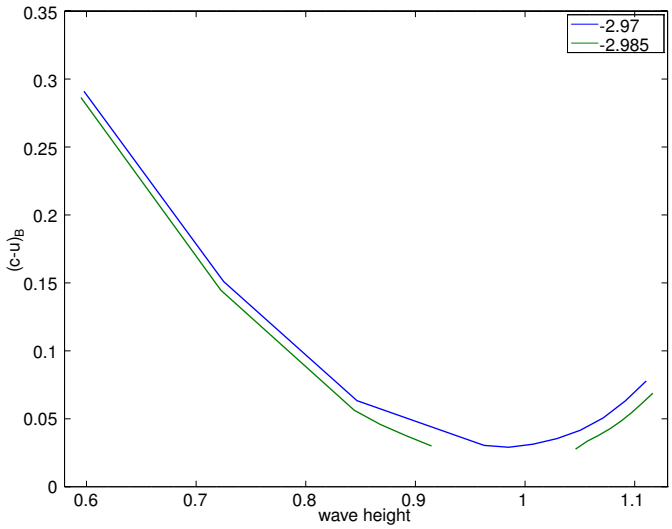

Figure 12: $(c-u)_B$ along the solution curve $\mathcal{C}$, parametrized by the wave height.

4.2 Critical vorticity and below

The presented procedure does not compute a maximal wave with a sharp angle at the top for all constant vorticities. In particular, if the vorticity is below γ_{crit}, it breaks down earlier. This behaviour was also observed in [38, 39] and attributed to a stagnation point at the bottom of the wave. An indication for this, is the value of $(c-u)$ at the bottom right below the crest which is close to zero, see Figure 7. This value is denoted by $(c-u)_B$, and is readily available, once the wave is computed, from the expression

$$(c-u)_B = \frac{1}{h_p\,(0, p_0)}.$$

A more detailed consideration revealed that for vorticities close to but greater than the critical value, $(c-u)_B$ has a minimum inside the bifurcation curve $\mathcal{C}$. Indeed, in Figure 12, we observe this behaviour of $(c-u)_B$ as a function of the continuation parameter, for two different values of vorticity. It is worth-mentioning that this behaviour of $(c-u)_B$ is common for all constant vorticities we considered. This observation motivated the idea that for vorticities smaller than the critical value, $(c-u)$ at the bottom should increase after the presumptive stagnation point, and thus the corresponding wave be computable with the presented algorithm.

The major obstacle in computing these waves is that intermediate steps along $\mathcal{C}$ are not computable. Instead, we consider some γ_0 above the critical value and compute the solution with maximum value of Q along $\mathcal{C}_{\gamma_0}$. Then we fix Q and instead consider γ as the bifurcation parameter, looking for a solution for $\gamma_1 < \gamma_{\text{crit}} < \gamma_0$. Now we switch back to Q as the bifurcation parameter and compute the upper section of $\mathcal{C}_{\gamma_1}$, bounded

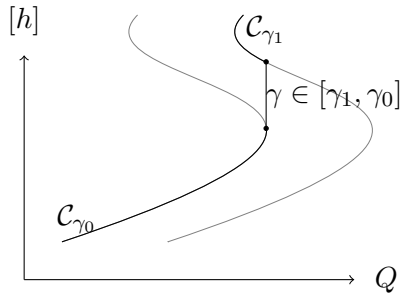

Figure 13: Numerical continuation via Q and γ combined

above by the wave of maximal wave height and below by the wave with the stagnation point at the bottom. This procedure is sketched in Figure 13.

Numerical experiments show that this approach works and that waves with stagnation point at the top exist even for vorticities below the critical value, see Figure 14. The results also show that the non-computable section of $\mathcal{C}$ grows larger even for small changes in γ. We emphasize the fact that this section of $\mathcal{C}$ is bounded, below and above, by two values of the bifurcation parameter Q, which give two *different* waves with stagnation points at the bottom; in Figure 16 we observe that the second wave is larger and steeper. Soon, the computable upper section of $\mathcal{C}$ becomes too small and it is practically incomputable with this scheme; the last wave we could compute was at $\gamma = \gamma_\ell = -3.062$. In summary, the γ-continuation technique in the interval $(\gamma_\ell, \gamma_{\text{crit}})$, indicates the existence of waves that have a stagnation point on the free surface, for vorticities *below* the critical value and conjectures the existence of waves with stagnation points both at the crest and at the bottom, right below the crest. This becomes transparent in Figure 17, where we present the basic characteristics of the maximal water wave with vorticity close to γ_ℓ; note that in this figure we present only the upper (new) part of the bifurcating diagram in order to display more details of this.

We recall that the knowledge of the pressure at the bottom is important for reconstruction of the waves, both analytically and experimentally, and that the pressure is readily available by equation (15).

We emphasize the fact that the pressure of the fluid displays a qualitative change for values of vorticity smaller than the critical value. Indeed, in Figure 8, where we depict the pressure of the fluid at the bottom, we see that when $\gamma < \gamma_{\text{crit}}$, the pressure at the point right below the crest displays a 'plateau' behaviour instead of a local maximum, which characterizes flows with $\gamma > \gamma_{\text{crit}}$. We observe this behaviour of the pressure at the bottom for the various numerical experiments that we have performed, and we have not included here for matters of brevity. An overview of these results is presented in Figure 11.

An indication of the occurrence of this 'plateau' can be given by studying the value of $P_{qq}(0, p_0)$, which should vanish; in Figure 9 we observe this behaviour of the quantity

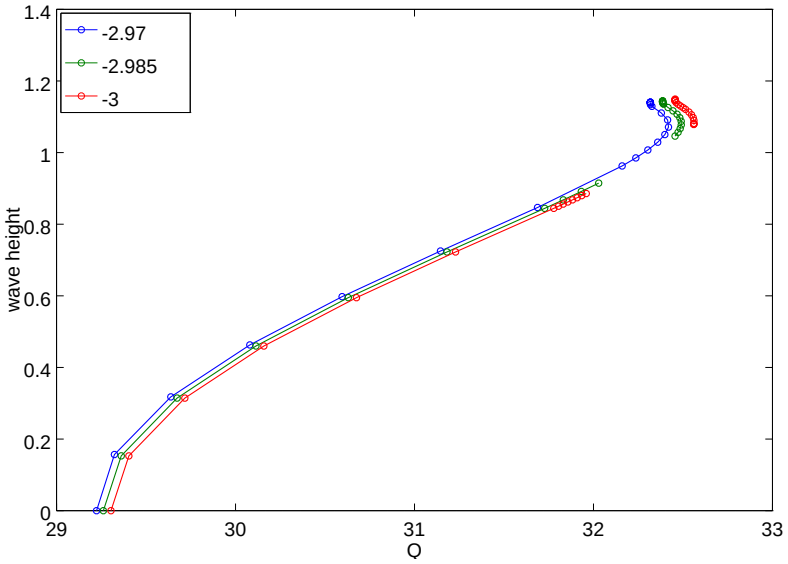

Figure 14: Bifurcation diagram for different values of constant vorticity in the interval $(\gamma_\ell, \gamma_{\text{crit}}]$.

$P_{qq}(0, p_0)$ for $\gamma = \gamma_{\text{crit}}$, around the neighbourhood of the point on the bifurcation curve where the gap will appear, namely Q_G.

A more detailed analysis of the features of the pressure shows that, if $\gamma_{\text{crit}} < \gamma < \gamma_\ell$, then this behaviour occurs for the two waves which correspond to the endpoints of the gap in the bifurcation curve. In Figure 10 we depict two waves which display this 'plateau' for two different values of constant vorticity, i.e. $\gamma = \gamma_{\text{crit}}$ and $\gamma = \gamma_\ell$. It is worth noting that these waves were obtained for substantially different points on the bifurcation curve, namely Q_G and Q_M, resulting different features: the latter one has a stagnation point at the top whereas the first one has a smooth surface.

For vorticities $\gamma < \gamma_\ell$ we are only able to compute the lower section of $\mathcal{C}$. The last computable wave has a smooth surface and instead a very small value of $(c - u)$ at the bottom, indicating a stagnation point there, see Figure 18. Moreover, the pressure distribution at the bottom for the last computable wave displays the above mentioned 'plateau' behaviour.

Gathering the results of the above procedure, for different values of constant vorticity, we display the wave height and average depth for maximal waves in Figure 19.

Remark 2. *We observed that the value of γ_{crit} is increasing as $|p_0|$ increases. However, not for all values of p_0 we can find γ_{crit}. Considering the case $\gamma < 0$, and following the discussion of Section 3 in [18], for given p_0 there is a minimum value of γ for which a bifurcation point (and a bifurcation curve) exists; we denote this value by γ_m. Moreover, it is shown that as $|p_0|$ increases, γ_m approaches zero rapidly. There is some (large enough) value of $|p_0|$ for which the γ_{crit} is equal to γ_m. In our case this value is $|p_0| \approx 4.4$, and for values of $|p_0|$ larger than that, waves do not display the feature of*

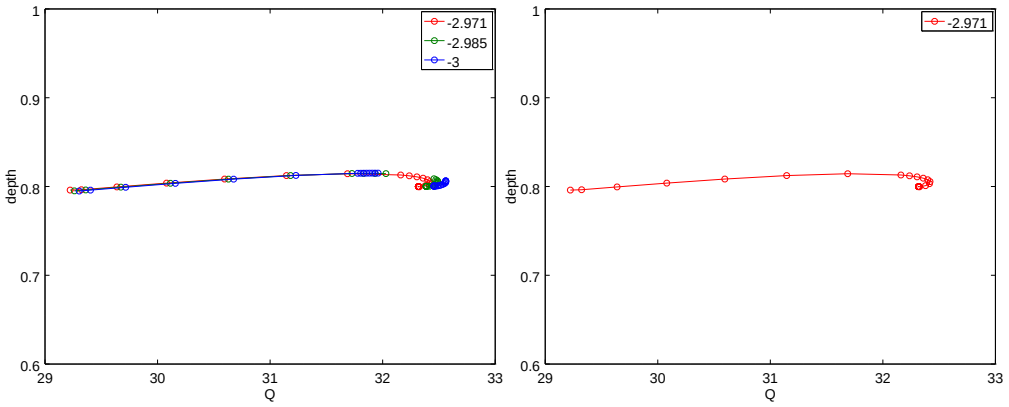

(a) Overlayed vorticities

(b) $\gamma = -2.971$

(c) $\gamma = -2.985$

(d) $\gamma = -3$

Figure 15: Depth along the bifurcation curve for two vorticities with a gap and γ_{crit}

critical vorticity. These results are in qualitative agreement with [39].

4.3 Examples of non-constant vorticity

An interesting case of non-constant vorticity is the case of vorticity varying linearly with respect to the stream function. A plethora of theoretical results is presented in several recent works. Existence for a variety of families of waves with critical layers is shown in [27, 26, 1], using arguments from bifurcation theory. Moreover, qualitative results for small amplitude waves are presented therein; analogous results for modal waves are presented in [28].

We consider the following distribution of vorticity:

$$\gamma(-p) = -a_1 p + a_0,$$

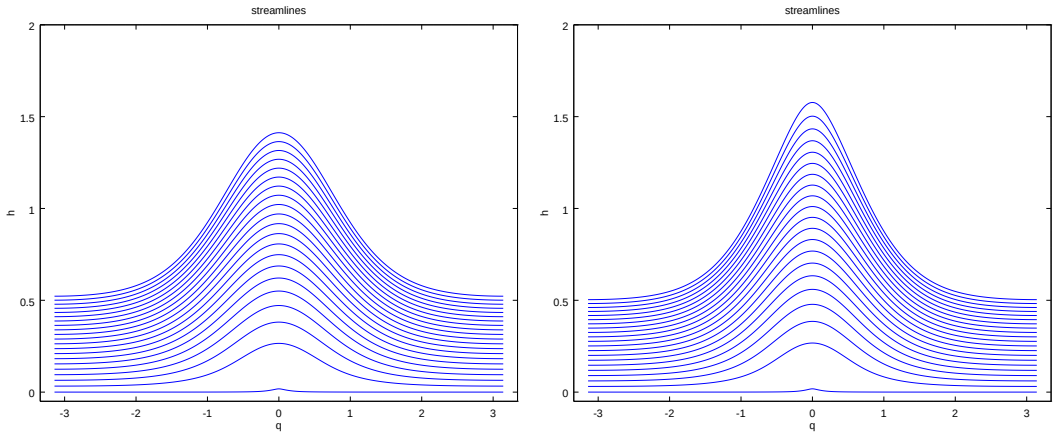

(a) Below the gap (b) Above the gap

Figure 16: Streamline for $\gamma = -3$ just below and above the gap.

then the laminar solution is given by

$$H(p;\lambda) = \int_{p_0}^{p} \frac{1}{\sqrt{\lambda - 2\Gamma(s)}} ds = \int_{p_0}^{p} \frac{1}{\sqrt{\lambda + a_1 s^2 - 2a_0 s}} ds.$$

The dispersion relation as given in [37] reads

$$\lambda^* + a_0\sqrt{\lambda^*} F(H(0;\lambda^*) - gF(H(0;\lambda^*)) = 0$$

with

$$F(d) = \begin{cases} \frac{\tanh(d\sqrt{1+a_1})}{\sqrt{1+a_1}} & \text{if } a_1 > -1 \\ d & \text{if } a_1 = -1 \\ \frac{\tan(d\sqrt{-(1+a_1)})}{\sqrt{-(1+a_1)}} & \text{if } a_1 < -1 \end{cases}.$$

We consider $\gamma_\alpha(-p)$ such that $\gamma_\alpha(-p_0) = 0$ and $\gamma_\alpha(0) = \alpha$ for $\alpha \in \{-1, 0, 1\}$. The analysis of this particular class of examples was motivated by the discussion in [38], where it is mentioned that, from experiments, wind typically has the effect of producing vorticity in the water near the surface. Thus, we discuss a case of non-constant, continuous distribution of vorticity, which vanishes at the bottom, but not at the surface of the fluid. Note, also, that $\alpha = 0$ is the case of a constant zero vorticity which gives us the Stokes' wave as the limiting wave, and we include it here, for comparison with the linear vorticity case.

Similarly to the case of constant vorticity we observe two turning points in Q and monotonously increasing wave heights for $\alpha \in \{-1, 0, 1\}$. Figures 20, 21 and 22 show some characteristics of the wave profile, in particular the free boundary, the velocity $(c - u)$ on the vertical line below the crest and the water pressure at the bottom, respectively, for the different values of α. We note that for the two last quantities we used equation

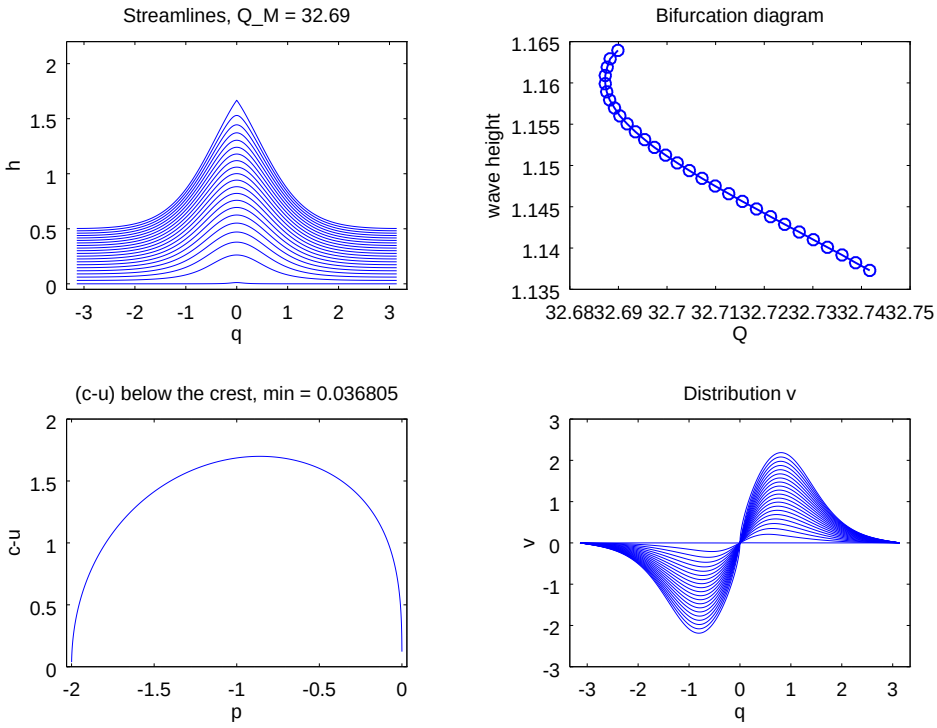

Figure 17: Wave for $\gamma = -3.05$ (obtained at $Q = Q_M$) and its bifurcation diagram.

(14) and (15). In summary we can say that the considered waves display similarities with waves of constant vorticity.

Finally, we have computed a wave for which the vorticity is linearly distributed, taking the value $\alpha = -10$ at the free surface and vanishes at the bottom, see Figure 23. For this wave, we observe a different behaviour from the waves of negative constant vorticity $\gamma < \gamma_\ell = -3.062$. Firstly, the wave with linearly distributed vorticity displays a stagnation point at the free surface, while the others display a stagnation point at the bottom. Secondly, the bifurcation curve has two turning points before it reaches a flow with stagnation point. Thirdly, and most striking, the wave with this non-constant vorticity, has a significantly larger wave height compared with other waves with constant negative vorticity.

Finally, we present the results for three more examples of non-constant vorticity in Figure 24. Here the vorticity distributions are either linear or quadratic with respect to the stream function and vanish on the bottom while at the free surface it holds $\gamma(0) = -4$. The three considered vorticity functions are

$$\gamma_\ell(-p) = -4\left(1 - \frac{p}{p_0}\right), \quad \gamma_a(-p) = -4\left(1 - \frac{p}{p_0}\right)^2 \quad \text{and} \quad \gamma_b(-p) = -4\left(1 - \frac{p^2}{p_0^2}\right).$$

Note that it holds $\gamma_b(-p) < \gamma_\ell(-p) < \gamma_a(-p)$ for $p \in [p_0, 0]$. Figure 24 shows the streamlines, as well as $c - u$ below the crest, for a wave near stagnation, for all three

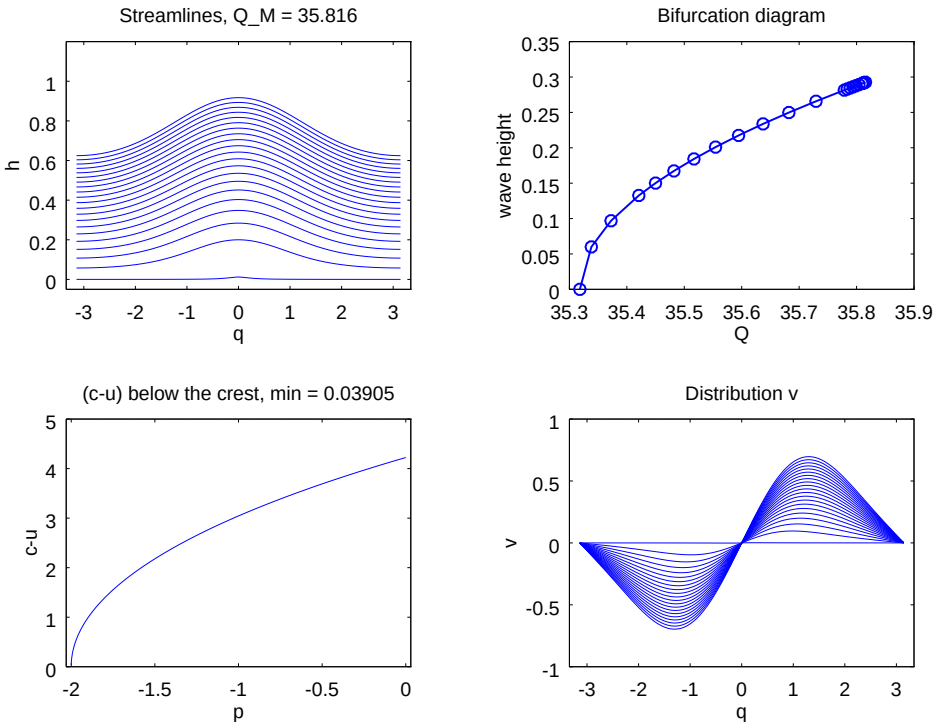

Figure 18: Wave for $\gamma = -5$ (obtained at $Q = Q_M$) and its bifurcation diagram.

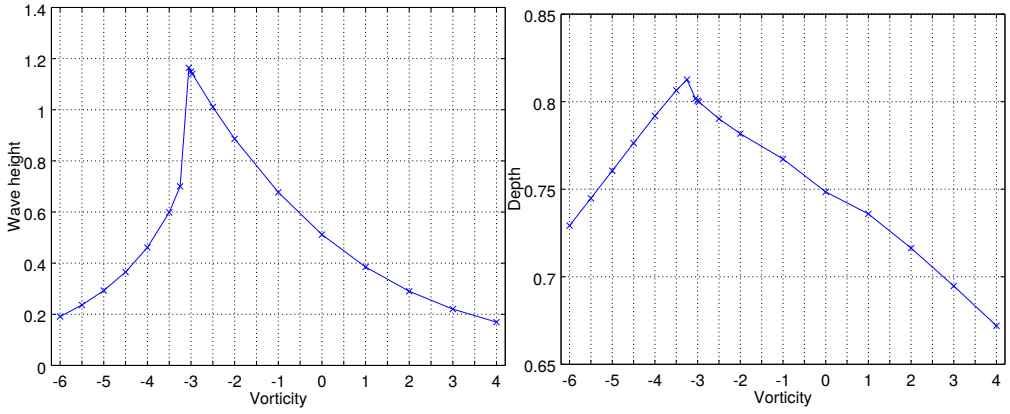

(a) Wave height. (b) Depth

Figure 19: Characteristic of the limiting wave for constant vorticity.

vorticity functions. It is notable that the wave height is inversely correlated with the point wise values of the vorticity functions, i.e. γ_a leads to the smallest and γ_b to the largest wave height.

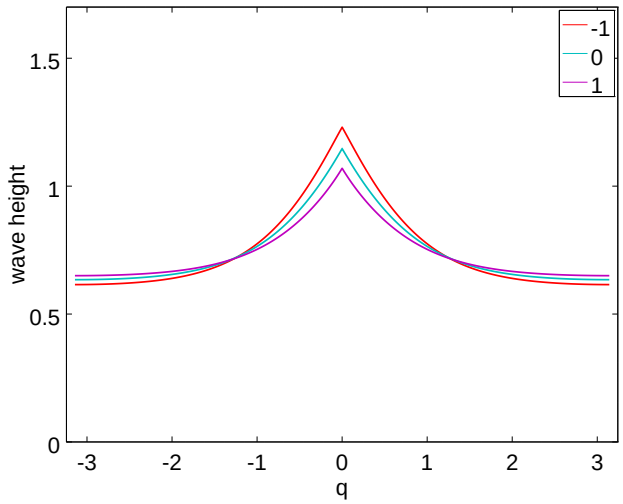

Figure 20: The free boundary for linear vorticity with $\gamma_\alpha(0) = \alpha \in \{-1, 0, 1\}$.

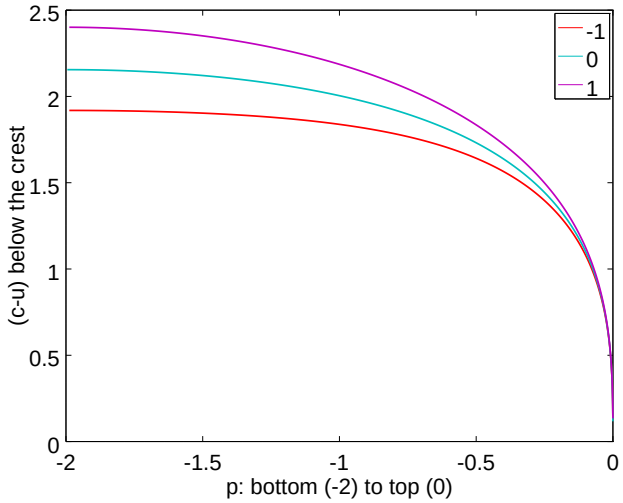

Figure 21: The velocity $(c - u)$ below the wave crest for linear vorticity with $\gamma_\alpha(0) = \alpha \in \{-1, 0, 1\}$.

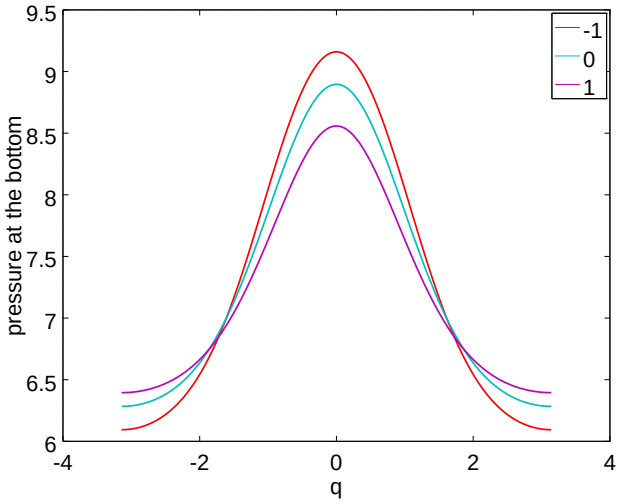

Figure 22: The pressure at the flat bottom for linear vorticity with $\gamma_\alpha(0) = \alpha \in \{-1, 0, 1\}$.

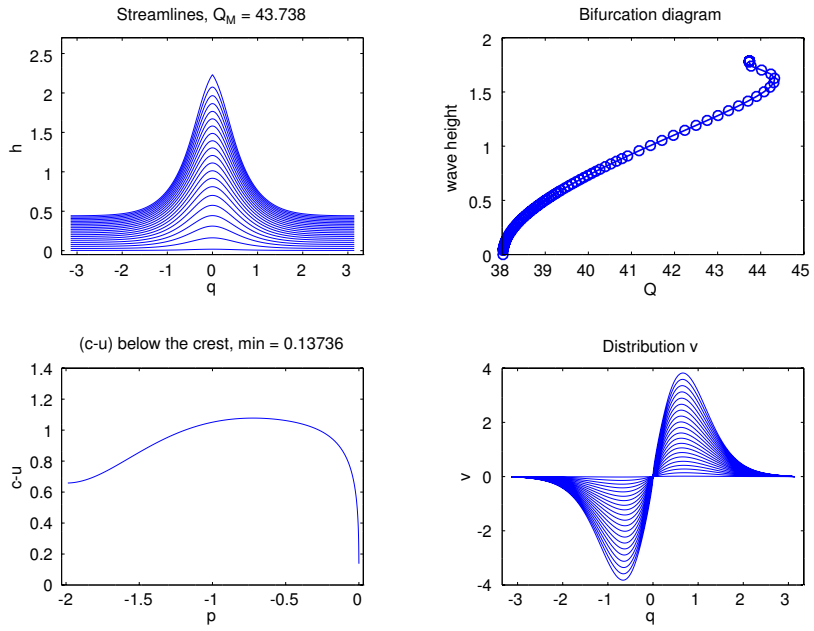

Figure 23: The water wave for linear vorticity $\gamma_\alpha(0) = \alpha = -10$.

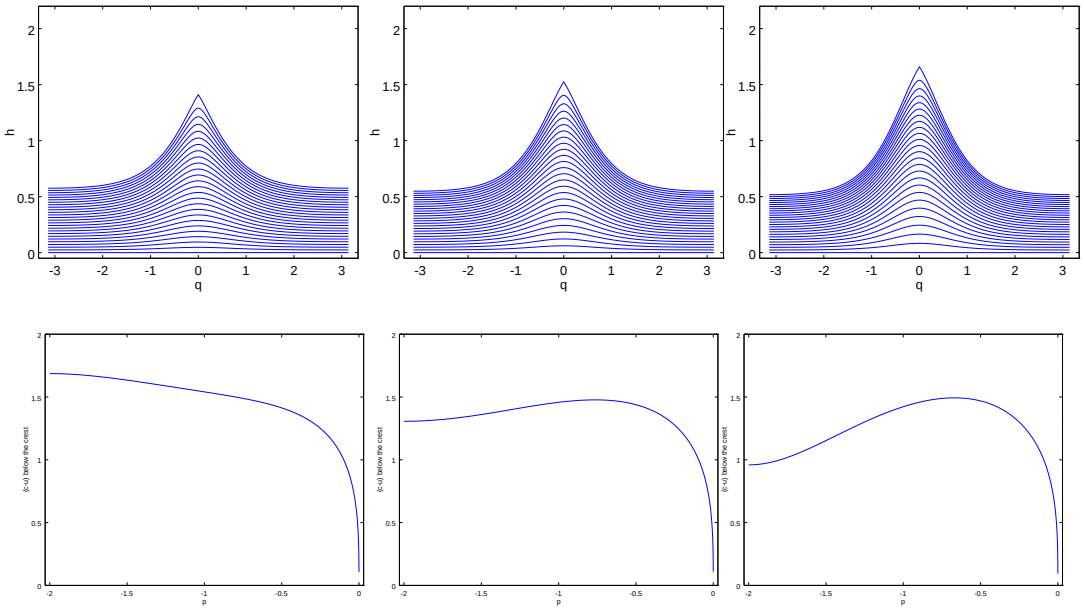

(a) $\gamma_a(-p) = -4\left(1 - \frac{p}{p_0}\right)^2$ (b) $\gamma_\ell(-p) = -4\left(1 - \frac{p}{p_0}\right)$ (c) $\gamma_b(-p) = -4\left(1 - \frac{p^2}{p_0^2}\right)$

Figure 24: Streamlines and $(c-u)$ below the crest for waves near stagnation for three quadratic vorticities with $\gamma(0) = -4$ and $\gamma(-p_0) = 0$.

5 Conclusions

We presented a detailed analysis of a numerical continuation algorithm to compute water waves. Using this algorithm, we rederived known results, with some results closer to stagnation points, as well as computed new characteristics of the waves, with the most important being:

- A new part of the branch of the bifurcation diagram.
- Limiting waves near stagnation, for the constant vorticity case, with new characteristics; see Section 4.2 for more details.
- Maximal waves of much larger amplitude for the case of linear vorticity.

Finally, we showed the performance of the algorithm for some cases of variable vorticity. A more systematic study of the case of general vorticity, through this algorithm, will be presented in future work.

Acknowledgements

The authors were supported by the project *Computation of large amplitude water waves* (P 27755-N25), funded by the Austrian Science Fund (FWF). We would like to thank A.

Constantin and O. Scherzer for the fruitful conversation both at the analytical and the numerical parts of this work. We also would like to sincerely thank the reviewers for their important suggestions and their constructive criticism, as those insightful comments led to a significant improvement on the presentation of our work.

References

[1] A. Aasen and K. Varholm. Traveling gravity water waves with critical layers. *Journal of Mathematical Fluid Mechanics*, pages 1–27, 2017.

[2] M. Ablowitz, A. S. Fokas, and Z. Musslimani. On a new non-local formulation of water waves. *Journal of Fluid Mechanics*, 562:313–343, 2006.

[3] E. L. Allgower and K. Georg. *Introduction to numerical continuation methods*, volume 45. SIAM, 2003.

[4] A. C. Ashton and A. S. Fokas. A non-local formulation of rotational water waves. *Journal of Fluid Mechanics*, 689:129–148, 2011.

[5] S. Balay, S. Abhyankar, M. F. Adams, J. Brown, P. Brune, K. Buschelman, L. Dalcin, V. Eijkhout, W. D. Gropp, D. Kaushik, M. G. Knepley, L. C. McInnes, K. Rupp, B. F. Smith, S. Zampini, H. Zhang, and H. Zhang. PETSc Web page. `http://www.mcs.anl.gov/petsc`, 2016.

[6] B. Buffoni and J. Toland. *Analytic theory of global bifurcation*. Princeton University Press, 2003.

[7] W. Choi. Nonlinear surface waves interacting with a linear shear current. *Mathematics and Computers in Simulation*, 80(1):29–36, 2009.

[8] D. Clamond. New exact relations for easy recovery of steady wave profiles from bottom pressure measurements. *Journal of Fluid Mechanics*, 726:547–558, 2013.

[9] D. Clamond and A. Constantin. Recovery of steady periodic wave profiles from pressure measurements at the bed. *Journal of Fluid Mechanics*, 714:463–475, 2013.

[10] A. Constantin. The trajectories of particles in stokes waves. *Inventiones mathematicae*, 166(3):523–535, 2006.

[11] A. Constantin. *Nonlinear Water Waves with Applications to Wave-Current Interactions and Tsunamis*, volume 81. SIAM, 2011.

[12] A. Constantin. Estimating wave heights from pressure data at the bed. *Journal of Fluid Mechanics*, 743:R2, 2014.

[13] A. Constantin, M. Ehrnström, E. Wahlén, et al. Symmetry of steady periodic gravity water waves with vorticity. *Duke Mathematical Journal*, 140(3):591–603, 2007.

[14] A. Constantin and J. Escher. Symmetry of steady periodic surface water waves with vorticity. *Journal of Fluid Mechanics*, 498:171–181, 2004.

[15] A. Constantin and J. Escher. Analyticity of periodic traveling free surface water waves with vorticity. *Annals of Mathematics*, pages 559–568, 2011.

[16] A. Constantin, K. Kalimeris, and O. Scherzer. Approximations of steady periodic water waves in flows with constant vorticity. *Nonlinear Analysis: Real World Applications*, 25:276–306, 2015.

[17] A. Constantin, K. Kalimeris, and O. Scherzer. A penalization method for calculating the flow beneath traveling water waves of large amplitude. *SIAM Journal on Applied Mathematics*, 75(4):1513–1535, 2015.

[18] A. Constantin and W. Strauss. Exact steady periodic water waves with vorticity. *Communications on Pure and Applied Mathematics*, 57(4):481–527, 2004.

[19] A. Constantin and W. Strauss. Rotational steady water waves near stagnation. *Philosophical Transactions of the Royal Society of London A: Mathematical, Physical and Engineering Sciences*, 365(1858):2227–2239, 2007.

[20] A. Constantin and W. Strauss. Pressure beneath a stokes wave. *Communications on Pure and Applied Mathematics*, 63(4):533–557, 2010.

[21] A. Constantin and E. Varvaruca. Steady periodic water waves with constant vorticity: regularity and local bifurcation. *Archive for rational mechanics and analysis*, 199(1):33–67, 2011.

[22] A. T. Da Silva and D. Peregrine. Steep, steady surface waves on water of finite depth with constant vorticity. *Journal of Fluid Mechanics*, 195:281–302, 1988.

[23] B. Deconinck and K. Oliveras. The instability of periodic surface gravity waves. *Journal of Fluid Mechanics*, 675:141–167, 2011.

[24] E. J. Doedel. *Numerical Continuation Methods for Dynamical Systems: Path following and boundary value problems*, chapter Lecture Notes on Numerical Analysis of Nonlinear Equations, pages 1–49. Springer Netherlands, Dordrecht, 2007.

[25] M.-L. Dubreil-Jacotin. Sur la détermination rigoureuse des ondes permanentes périodiques d'ampleur finie. *Thèses françaises de l'entre-deux-guerres*, 160:1–75, 1934.

[26] M. Ehrnström, J. Escher, and G. Villari. Steady water waves with multiple critical layers: interior dynamics. *Journal of Mathematical Fluid Mechanics*, pages 1–13, 2012.

[27] M. Ehrnström, J. Escher, and E. Wahlén. Steady water waves with multiple critical layers. *SIAM Journal on Mathematical Analysis*, 43(3):1436–1456, 2011.

[28] M. Ehrnström and E. Wahlén. Trimodal steady water waves. *Arch. Ration. Mech. Anal.*, 216:449–471, 2015.

[29] J. Escher and B.-V. Matioc. Analyticity of rotational water waves. In *Elliptic and Parabolic Equations*, pages 111–137. Springer, 2015.

[30] A. S. Fokas and K. Kalimeris. Water waves with moving boundaries. to appear *in Journal of Fluid Mechanics*.

[31] A. S. Fokas and K. Kalimeris. A novel non-local formulation of water waves. In T. J. Bridges, M. D. Groves, and D. P. Nicholls, editors, *Lectures on the Theory of Water Waves*, pages 63–77. Cambridge University Press, 2016. Cambridge Books Online.

[32] A. S. Fokas and A. Nachbin. Water waves over a variable bottom: a non-local formulation and conformal mappings. *Journal of Fluid Mechanics*, 695:288–309, 2012.

[33] D. Henry. On the pressure transfer function for solitary water waves with vorticity. *Mathematische Annalen*, 357(1):23–30, 2013.

[34] D. Henry. Steady periodic waves bifurcating for fixed-depth rotational flows. *Quarterly of Applied Mathematics*, 71(3):455–487, 2013.

[35] D. Henry and A.-V. Matioc. Global bifurcation of capillary–gravity-stratified water waves. *Proceedings of the Royal Society of Edinburgh Section A: Mathematics*, 144(4):775–786, 2014.

[36] K. Kalimeris. Asymptotic expansions for steady periodic water waves in flows with constant vorticity. *Nonlinear Analysis: Real World Applications*, 2017.

[37] P. Karageorgis. Dispersion relation for water waves with non-constant vorticity. *European Journal of Mechanics-B/Fluids*, 34:7–12, 2012.

[38] J. Ko and W. Strauss. Effect of vorticity on steady water waves. *Journal of Fluid Mechanics*, 608:197–215, 2008.

[39] J. Ko and W. Strauss. Large-amplitude steady rotational water waves. *European Journal of Mechanics - B/Fluids*, 27(2):96 – 109, 2008.

[40] F. Kogelbauer. Recovery of the wave profile for irrotational periodic water waves from pressure measurements. *Nonlinear Analysis: Real World Applications*, 22:219–224, 2015.

[41] M. Longuet-Higgins and M. Tanaka. On the crest instabilities of steep surface waves. *Journal of Fluid Mechanics*, 336:51–68, 1997.

[42] D. V. Maklakov. Almost-highest gravity waves on water of finite depth. *European Journal of Applied Mathematics*, 13(1):67–93, 2002.

[43] B.-V. Matioc. Global bifurcation for water waves with capillary effects and constant vorticity. *Monatshefte für Mathematik*, 174(3):459–475, 2014.

[44] P. A. Milewski, J.-M. Vanden-Broeck, and Z. Wang. Dynamics of steep two-dimensional gravity–capillary solitary waves. *Journal of Fluid Mechanics*, 664:466–477, 2010.

[45] A. Nachbin and R. Ribeiro-Junior. A boundary integral formulation for particle trajectories in stokes waves. *Discrete Contin. Dyn. Syst*, 34:3135–3153, 2014.

[46] K. L. Oliveras, V. Vasan, B. Deconinck, and D. Henderson. Recovering the water-wave profile from pressure measurements. *SIAM Journal on Applied Mathematics*, 72(3):897–918, 2012.

[47] R. Ribeiro, P. A. Milewski, and A. Nachbin. Flow structure beneath rotational water waves with stagnation points. *Journal of Fluid Mechanics*, 812:792–814, 2017.

[48] L. Schwartz and J. Fenton. Strongly nonlinear waves. *Annual review of fluid mechanics*, 14(1):39–60, 1982.

[49] R. Seydel. *Practical bifurcation and stability analysis*, volume 5. Springer Science & Business Media, 2009.

[50] J. A. Simmen and P. Saffman. Steady deep-water waves on a linear shear current. *Studies in Applied Mathematics*, 73(1):35–57, 1985.

[51] W. Strauss. Steady water waves. *Bulletin of the American Mathematical Society*, 47(4):671–694, 2010.

[52] G. Thomas. Wave–current interactions: an experimental and numerical study. part 2. nonlinear waves. *Journal of Fluid Mechanics*, 216:505–536, 1990.

[53] G. Thomas and G. Klopman. *Gravity Waves in Water of Finite Depth*, chapter Wave-current interactions in the near shore region, pages 255–319. Computational Mechanics Publications, 1997.

[54] E. Varvaruca. On the existence of extreme waves and the stokes conjecture with vorticity. *Journal of Differential Equations*, 246(10):4043–4076, 2009.

[55] V. Vasan and B. Deconinck. The inverse water wave problem of bathymetry detection. *Journal of Fluid Mechanics*, 714:562–590, 2013.

[56] V. Vasan and K. Oliveras. Pressure beneath a traveling wave with constant vorticity. *Discrete Contin. Dyn. Syst*, 34:3219–3239, 2014.

[57] E. Wahlén. Steady water waves with a critical layer. *Journal of Differential Equations*, 246(6):2468–2483, 2009.

[58] S. Walsh. Steady stratified periodic gravity waves with surface tension ii: global bifurcation. *Discrete Contin. Dyn. Syst*, 34(8):3287–3315, 2014.